Modelling the Energy Production of a Borehole Thermal Energy Storage (BTES) System

Jessica Maria Chicco * and Giuseppe Mandrone

Interuniversity Department of Regional, and Urban Studies, and Planning (DIST), University of Turin, 10125 Torino, Italy
* Correspondence: jessica.chicco@unito.it

Abstract: Geopolitical developments since February 2022 and the numerous debates on climate change such as the COP27 are pushing for a greater acceleration in decarbonising the energy sector. The use of geothermal energy for thermal energy production and storage in district heating and cooling (DHC) grids may also be a key element in overcoming short-term energy peaks. This work aimed at evaluating the efficiency and performance of one of the most promising underground thermal energy storage systems, which uses boreholes to store heat or cold (BTES). Numerical simulations allowed for understanding how these technologies can be used as backup systems, or when the energy demand overcomes that supplied by conventional heating systems. The knowledge on how to exploit this energy source shows that a continuous heat extraction from the storage volume can meet both the base and peak load requests for several users, with cumulative energy amounting to 476,000 kWh over the first month. This study proved how the integration of these technologies in DHC contexts can contribute to greater energy and economic savings, becoming an efficient and flexible solution to meet the energy demand from the grid, and also as a backup system.

Keywords: district heating; thermal energy storage; geothermal energy; numerical simulation

1. Introduction

The global energy demand is increasing as much as the population grows. The International Energy Association (IEA) reported a 5% rise over the last year, which was almost covered by fossil fuels, threatening to push CO_2 emissions from the power sector to records levels in 2022 [1]. The 2015 Paris Agreement aims to avoid the effects of climate change by looking at a global temperature rise of no more than 2 °C [2]. As well, in November 2021 during the United Nations Change Conference (COP26) held in Glasgow, the parties found solutions to lower emissions, increase resilience, and provide financial incentives [3]. These issues were also addressed in the recent COP27 held in Egypt in November 2022, identifying innovative solutions to investing in specific projects such as climate action plans [4]. Even though the recent energy crisis in 2022 made natural gas far more expensive, the relatively small increase in coal emissions has been considerably overcome by the great expansion of renewables such as solar or wind energies. This means that CO_2 emissions are growing far less quickly than expected, and policy actions are making important changes in the energy economy [5].

Aimed at satisfying the strong rebound in the energy demand and consumption, developing clean energy technologies is of paramount importance. In this context, energy production by renewables as well as the improvement of building energy efficiency can ensure a valuable solution, but they need to be more incentivised, requiring the engagement of corporates, stakeholders, policymakers, consumers, and prosumers. Renewable energy sources, energy efficiency, and the reduction of greenhouse gas (GHG)

emissions represent the three main pillars also underlined in the latest European directives such as the "European Green Deal" [6], which contribute to cutting GHG emissions by at least 55% by 2030. In this scenario, thermal energy sector for space heating and cooling accounts for approximately 50% of final energy needs, covering more than 25% of GHG emissions. However, this issue has not been dealt with well enough by politics in the past decade, showing strong weaknesses in the green and sustainable energy transition process [7]. Decarbonising the heating and cooling of buildings is still a great challenge, but it is essential since it shows a large potential for improving the overall energy efficiency. The strategies and guidelines compiled by the HRE4 study [8] for 14 EU countries, accounting for 80% of the heating and cooling demand, proved that sustainable decarbonisation of the European energy system could be developed through the provision of approximately 50% of the EU heat demands by 2050, supplying the remaining heat demands via heat pumps [9]. Among the renewables, geothermal energy represents a key technology ensuring better energy efficiency especially in the district heating and cooling (DHC) contexts, as also stated by HRE4.

This study focused on a numerical simulation of an underground storage system in the pre-Alpine foothills of Italy, as an implementation of conventional closed loop geothermal plants for civil uses. It aimed at evaluating the ground thermal behaviour as well as the surrounding environmental effects during the BTES operation, both in the storage and in the thermal energy extraction phases. Numerical simulations were hence conducted using commercial software (*Feflow; WASY DHI Group*) that was revealed to be very useful in defining BTES performances, such as BHE design and operational parameters, characterised by one of the most common thermo-technical solutions in specific hydrogeological and climatic contexts. Modelling of the BTES was possible thanks to specific hydrogeological and thermo-physical data from a real case study, while the heat production (from thermal solar or waste heat) was assumed as representative of the investigated geographical area but is not supported by measures.

2. Underground Thermal Energy Storage Systems

The green energy transition from fossil fuels to sustainable energy forms requires the large-scale storage of energy. Underground thermal energy storage (UTES) systems can be more efficient when combined with other sustainable and renewable energy sources such as geothermal energy, further developing smart energy grids. These systems represent a large challenge, because they allow optimising the gap between the thermal energy demand and supply seasonally, both for large areas and many consumers. Storage is currently the only way to use volatile renewables such as solar thermal, making use of waste heat to enhance the overall energy efficiency of the heating and cooling market, which is one of the EU's goals. The utilisation of UTES, as a knot for coupling and integration of decentralised renewable energy heat sources, contributes to the overall efficiency, flexibility, and response time of a DHC system; UTES can also be used to cover the peak demand load as well as to provide a backup supply [10]. The coupling of local renewable energy subsystems and installations to onsite thermal energy storage reduces the heat consumption of the system, without any physical connection to the main DHC network and enabling the share of renewable energies to grow massively [11]. Large-scale UTES allows reducing great amounts of GHG emissions by ensuring renewable heat at affordable prices all year round, since it is the cheapest way to store such large amounts of heat. The UTES technologies are divided in four main typologies, with the common feature of storing the surplus heat and cold (usually in large quantities and over several seasons or years). UTES also represents the best storage solution for temperature levels between less than 10 °C and up to 90 °C [7], using different kinds of storage such as subsurface (PTES), aquifers (ATES), borehole heat exchangers (BTES), abandoned coal mines (MTES) or rock caverns (CTES), as described in detail in [10]. Among these, BTES systems are becoming very popular because of their suitability for seasonal storage of thermal energy, thanks to their slow thermal response and large

storage capacities [12]. They usually consist of a field of borehole heat exchangers (BHEs) transferring heat with the surrounding rocks, predominantly by conduction [13], and require only a small amount of space to tap into a large volume of subsurface rocks at relatively low costs. These characteristics give them a great advantage with respect to other kinds of storage technologies. Other selling points include the fewer geographical limitations than the other typologies, as well as the fact that BTES systems are most effective when diurnal and seasonal storage are used in conjunction [14].

Several aspects can influence BTES operational features, such as the volume and capacity of the storage, the hydrogeological and thermo-physical properties of the ground [15], as well as the BHE configuration, their distance, length [16], and technical parameters [14]. All of these important aspects need to be understood in detail to improve the whole energy efficiency of the system. Few studies have focused on these features; in most cases, numerical models have focused on BTES performance and configuration, taking into account some of the thermo-physical parameters of the ground, considered as a homogeneous and isotropic medium [14–16]. Other works mainly addressed what modelling approach is the most appropriate for BTES [17]. Therefore, a detailed study of this field, such as a complete numerical modelling, is needed. This allows providing site selection and system design as well as highlighting the performances over the short and long term, increasing the economic viability of BTES technology.

3. Case Study

The study area is located in the Italian pre-Alpine foothills (Figure 1) where detailed geothermal information is available. This area is mainly characterised by a high morphological variability from soft to angular shapes, rounded slopes, mountain ridges, and little valleys. It is mountainous in the northern portion with a gentle decrease in the elevation towards the southern part until the Piedmont Plain [18,19].
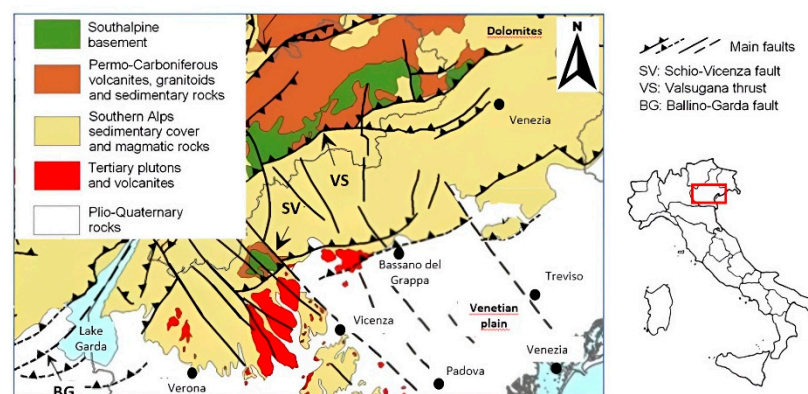

Figure 1. Geological sketch map of the study area (modified from [20]).

This geomorphological heterogeneity is mainly related to the multiphase Alpine tectonics [21], characterised by numerous crustal shortening events that occurred during the Alpine orogeny and by the Neogene and Quaternary compressive phases. In this sector, the Alps are composed of a Europe-verging collisional wedge (Alpine domain) and a south propagating fold-and-thrust belt (south Alpine domain) separated by a major fault system.

From a structural point of view, the pre-Alpine foothills form an EW trending fold-and-thrust belt with a main tectonic transport towards the south [22]. This portion also preserved the different paleogeographic units of the Mesozoic Adriatic passive margin, even if several crustal shortenings have been verified, and shows features consistent with shallow marine carbonate accumulation until the uppermost Early Jurassic, with predominantly shallow marine carbonate sediments, calcarenites, and marly carbonates [23–25]. The Neo-Alpine tectonic activity is characterised by south verging overthrusts

also involving the crystalline basement. During the rifting phase (Late Triassic), the Norian carbonate platform crumbled, producing high and low structural parts bordered by listric faults [26,27]. This created different sedimentary facies between the various structural sectors, which ended with a general subsidence of the whole area due to the opening of the Ligurian–Piedmont Oceanic Basin. Among these different structural sectors, the large carbonate platform, extending from the Po Plain to the extreme NE Italian portion, was characterised by two sedimentary phases with a deposition of grey to oolitic limestones [28]. These geological formations are in etheropy with dolomitic and marly limestones. Finally, between the Palaeocene/Oligocene and Miocene periods, the sedimentation of volcanic and subvolcanic sediments was verified [26,29].

From a hydrogeological point of view, the study area presents a very complex system. The hydrographic network varies greatly from constant and regular to discontinuous fluvial regimes, passing from the valley to the hill area.

The overall flow direction is marked by a principal vertical component through deep karst structures with channels and underground caves, sometimes reaching more than 1000 m of vertical gradient. This means a very deep groundwater flow, and therefore dry groundwater conditions at shallow depths such as those investigated in the present study [30,31].

4. Ground Response Test (GRT) and Back Analysis from a Real Case Study

When facing high energy demands, especially for residential or public buildings in DHC contexts, the number and design of the BHEs used both to extract and to store thermal energy have to be accurately defined. In such a case, with unknown information regarding the ground properties, specific surveys are needed in order to set the proper BHE configuration as well as their number, distance, and depth, ensuring a great energy efficiency and the successful functionality of the whole energy system. Among these specific surveys, the ground response test (GRT) is revealed to be very useful, aimed at better understanding the thermo-physical parameters of the underground soils. Usually, a conventional GRT provides measures of the inlet and outlet fluid temperatures inside the geothermal pipes (T_{in} and T_{out}, respectively) when it comes back to the machine, from which the equivalent thermal properties such as the ground thermal conductivity, the BHE thermal resistance, and the undisturbed ground temperature are obtained. However, these thermal parameters include the overall effect of the ground/aquifer/pipe system without well characterising the ground components from which the whole energy system depends. In this regard, a back analysis of a real GRT through a sensitivity procedure by using specific software is very useful in better defining the specific thermo-physical properties of the ground, ensuring a better BHE configuration and, thus, a greater efficiency of the overall energy system.

4.1. Interpretation of the Field GRT

An accurate interpretation of a GRT conducted in the study area was performed. The short time interval while recording the different parameters together with the long test duration (equal to 312 h more than the typical 72 h), allowed obtaining a high level of detail and, therefore, a greater accuracy of the real thermal exchange represented by the thermal conductivity and thermal resistance.

Two known methods consisting of specific equations were used and compared, aimed at better defining the obtained results.

The first method refers to that developed by [32] which is an outline of what was stated in [33] and introduced by Equation (1):

$$Tf(t) = \frac{q}{4\pi\lambda} * \left(ln\frac{4\alpha t}{r^2} - \gamma \right) + q * Rb + Tg \tag{1}$$

where (Table 1):

Table 1. List of parameters of the equation (1).

$Tf(t)$	Average fluid temperature (T_{in} and T_{out}) depending on the test time, expressed in °C
Q	Injected power per unit of length and time, expressed in W and derived from: $q = Q/H$ (where H is the drilling depth)
π	Equal to 3.14
λ	Ground thermal conductivity, expressed in W*m^{-1}K^{-1}
γ	Euler's constant equal to 0.5772
α	Thermal diffusivity, expressed in m²/s
t	Test time, expressed in s
r	Borehole radius, expressed in m
Rb	Thermal resistance of the ground/fluid/pipe system, expressed in K/(W/m)
Tg	Undisturbed temperature, expressed in °C

The second one concerns the equations elaborated by [34], which details the value *g* as the function representing the thermal response factor for a single pipe or for different configurations, as expressed in Equation (2):

$$Tf = Tg - qRb - \frac{q}{2\pi\lambda} g \left(\frac{t}{tsc}, \frac{r}{H} \right) \qquad (2)$$

where:

g is a function representing the response thermal factor for a single pipe or for different configurations.

It depends on:

- t/ts, where *t* is the time expressed in s;
- $ts = H^2/9\alpha$.

The results from the GRT interpretation using the two methods allowed obtaining an equivalent value of the thermal conductivity and of the thermal resistance of the ground/aquifer/pipe system. In addition, the thermal resistance was evaluated using the method in [35] reviewed from [36].

4.2. Back Analysis of the GRT Field Test, through Numerical Simulations

One of the most able software to model all of the relevant components of the heat transfer process thanks to its flexible meshing strategies is FeFlow software (Wasy DHI Group) [37]. Closed loop geothermal systems for thermal energy production as well as borehole thermal energy storage (BTES) technologies for storing heat and cold can be simulated at different levels of detail until fully discretised solutions are found. This software allows obtaining interesting results regarding thermal exchange, considering each part of the ground/aquifer/pipe system; it also enables the achievement of a detailed value of the thermal power extraction. This high degree of detail is due to the possibility of introducing specific boundary conditions such as "borehole heat exchangers BC", "hydraulic head BC", and "temperature BC", providing a very detailed representation of the BHE with a high level of numerical efficiency.

The back analysis of the GRT previously conducted in real conditions consisted of an accurate sensitivity analysis by the Feflow software. The input values used during the real GRT together with the hydrogeological parameters derived from the literature and previous field surveys (Table 1) were put in the numerical model. The geometrical domain was characterised by five layers at different depths, in a 15 × 15 × 100 mesh in which a punctual element was placed. The punctual element represents a typical BHE, 100 m in depth, and equipped with a double U geothermal pipe. As presented in [37],

during the numerical simulation a series of specific calculations with a high accuracy were set.

The specific field and laboratory surveys in the study area consisting of rock coring and Lugeon and Le Franc tests revealed a detailed stratigraphic profile as summarised in Table 2.

Table 2. Lithological characteristics of the underground lithologies, as revealed by specific field and laboratory surveys in the study area.

Lithology	Depth (m)	Hydraulic Conductivity (K, m/d)	Porosity (θ, %)	Temperature (°C)	Groundwater Level (m)
Sandy, clayey sediments	From 0 to −15	0.864	30	14	−100
Marly limestones	From −15 to −25	0.864	5	14	−100
Limestone	From −15 to −100	0.0864	5	14	−100

The final input values of the real GRT (T_{in} and T_{out}) were approached as close as possible by progressively changing the thermal conductivity of the three main underground lithologies (Table 3), as the most variable thermal property; a constant thermal energy power equal to 8500 W and an undisturbed temperature of 14 °C for the whole domain were also fixed.

This sensitivity analysis was revealed to be very useful for better understanding the thermal conductivity values as well as the main ground parameters and allowed for the calibration of the hydrogeological and thermo-technical models. Among the obtained results, the parameters from "back analysis 1" were used because they were closest to the real data.

The row data from the real and simulated GRTs are represented in Figure 2.

Table 3. Input data from the real GRT compared with the three back analyses. Numerical simulations in the back analysis were carried out by progressively changing the thermal conductivity of the different underground lithologies (see Table 1). Key: T_{in} and T_{out} are the inlet and outlet temperatures of the fluid through pipes; λ is the thermal conductivity.

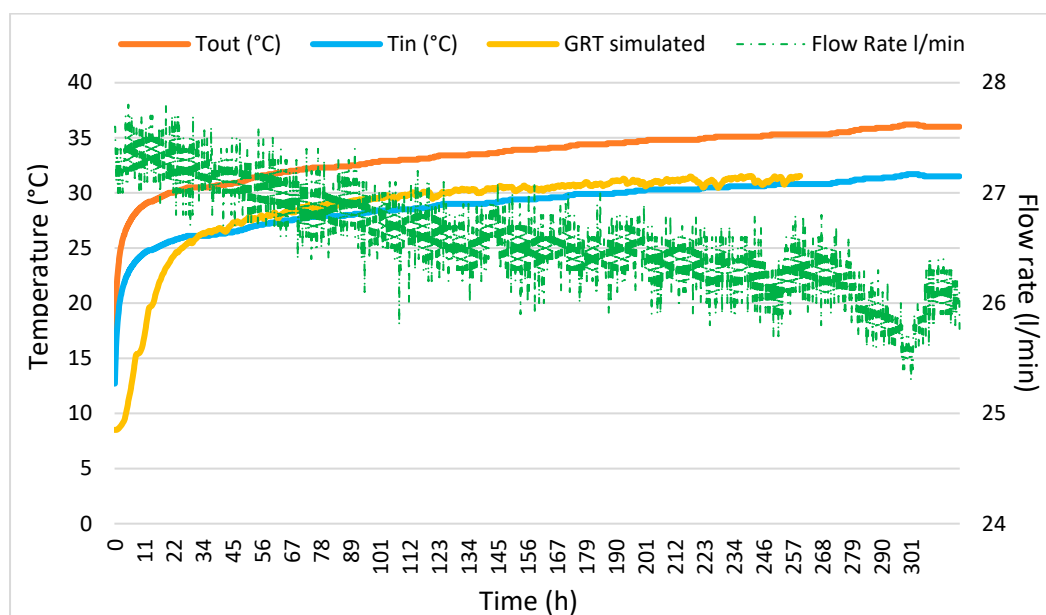| Test	T_{in} (°C)	T_{out} (°C)	λ (W*m^{-1}K^{-1})	Lithologies
GRT	36.0	31.5	2.52	All domains
Back analysis 1	36.1	31.5	0.37	Sandy clay
			1.37	Marly limestone
			2.67	Limestone
Back analysis 2	36.2	31.5	0.38	Sandy clay
			1.38	Marly limestone
			2.68	Limestone
Back analysis 3	38.6	35.8	0.42	Sandy clay
			1.42	Marly limestone
			2.72	Limestone

Figure 2. Obtained results from the GRT in real conditions: inlet (T_{in}, °C) and outlet (T_{out}, °C) temperatures vs. flow rate (l/min), over 13 days of the field test duration. A comparison with the simulated GRT (over the same period, but with a shorter time interval) is also shown.

5. Numerical Model Setup for a BTES Plant

As previously described (Section 4.2), FeFlow allows joining together the thermotechnical characteristics of a BHE (e.g., the inner and outer pipe diameter, the characteristics of the fluid through pipes, and the grouting mixture) together with hydrogeological and lithological characteristics. This was revealed to be very important in modelling how the underground behaves when BHEs are used both as storage during the summer season and for extraction of the stored heat in colder months. Furthermore, the numerical simulations allowed setting the right number of BHEs, their distance, and depth, as well as the array configuration. Therefore, using geometrical, groundwater, and heat transport models as closely as possible to the real conditions is of paramount importance.

5.1. Geometrical Model

A triangular super mesh was ascribed to the model, because of its ability to reproduce complex shapes as well as to easily change the level of refinement. In this case, a specific global refinement of the entire mesh was conducted, setting up 0.2 m for polygons and the point target size, as well as a point gradation of 2. Aimed at avoiding irregular-shaped elements and obtuse-angled triangles, a further mesh smoothing was performed. A check for obtuse angles and triangles violating the Delaunay criterion was also realised.

The Algebraic MultiGrid Solver (SAMG) was used, because it is the fastest and more robust equation solver for complex meshes. It allows for a fast convergence, and it is efficient for typical problems over a wide range of applications. Its main advantage is its parallelisation on a multicore system, as well as its more efficient solution algorithm [38].

The calculations were computed on each active node of the finite element mesh and interpolated within them. The denser the mesh, the better is the numerical accuracy. The local refinement around the BHE was conducted during its generation to obtain a greater mesh quality. Once the model was discretised in 2D, it was extended into a 3D model with prismatic elements through the use of the "3D layer configuration" tool. The modelled area was built as a prism of 50 × 50 × 80 m, divided by a total of 5 slices at different depths from the ground level to −80 m (Figure 3). The slices were set at the ground level,

and −15, −25, and −60 m according to the hydrogeological characteristics derived from the literature and specific field studies. The layer at −60 m represented the BHE bottom beyond which a further layer at −80 m was placed, to investigate how the ground behaved under the BHEs and if it was affected during their operation (Figure 3).
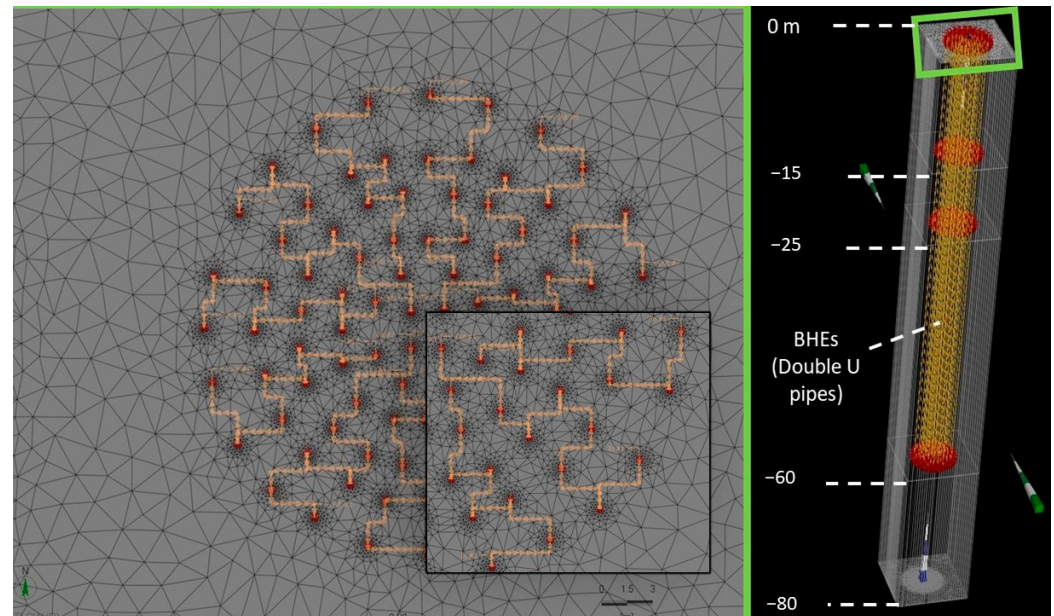

Figure 3. Geometrical model of the BTES. On the left is the horizontal section where the red points represent boreholes and the yellow lines show the 12 circuits, each one consisting of 8 BHEs (see the zoomed-in inset). On the right, the 3D domain is divided by 5 slices at different depths (from the ground level to −80 m in depth), 20 m more than the BHEs' length.

Ninety-six punctual elements were set, forming a cylinder of approximately 30 m in diameter. A finer discretised mesh was made around them to refine the model. Each of them simulated a BHE equipped with double U geothermal pipes. The BHEs were spaced 2 m in the inner part of the circle while progressively extending until spaced at 3 m for the more external circles. These are typical distances to minimise thermal losses, ensuring a good thermal energy storage. Furthermore, 12 symmetrical arrays composed of eight BHEs each and representing the fluid circuits during the plant operation were realised.

5.2. Geological Model

Based on data achieved from field and laboratory surveys as summarised in Table 1, and thanks to the right value for the thermal conductivity obtained through the back analyses of the GRT (Section 4.2), hydrogeological and thermal models were also set (Figure 4).
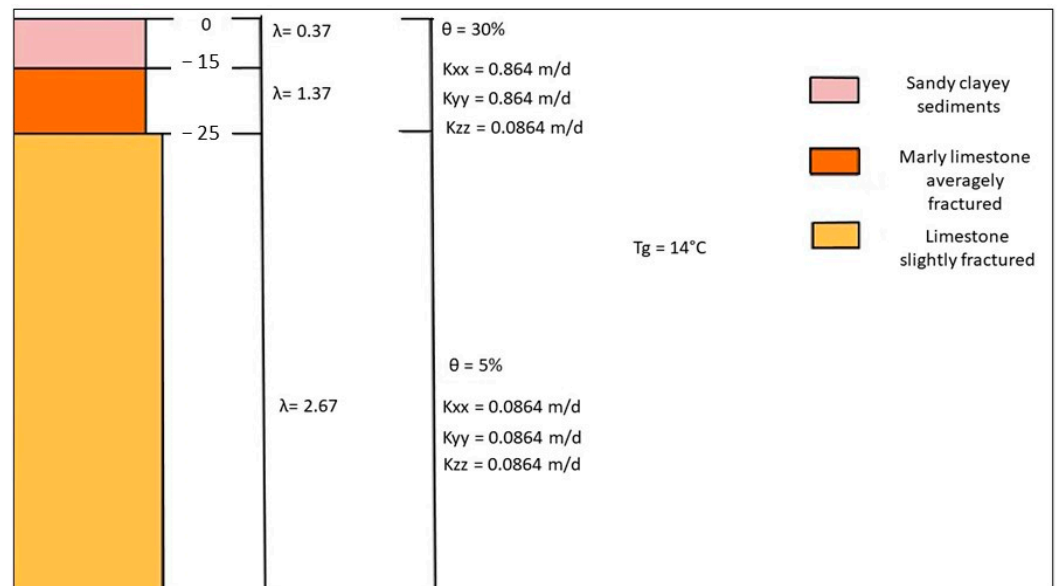
Figure 4. Hydrogeological and thermo-physical input parameters used for the numerical simulation.

The hydrogeological model was the first calibrated to achieve hydraulic heads as close as possible to real values (Table 2). At first, the calibration was conducted in steady-state groundwater conditions to obtain the right inputs for a transient state modality.

The investigated area is characterised by deep karst aquifers meaning dry groundwater conditions at shallow depths. Boundary conditions such as "hydraulic BC" were hence applied to the whole domain, in order to well define the absence of the groundwater flow in the numerical simulation and to allow the software to work in dry conditions.

Based on the information from field studies, as reported in Tables 1 and 2, as well as from the literature, the hydraulic and thermo-physical parameters of the underground lithologies used for the hydrogeological and thermo-physical models are summarised below, and clearly represented in Figure 4:

- groundwater level (not detected);
- undisturbed ground temperature (T);
- thermal conductivity of the ground (λ);
- hydraulic conductivity along the three directions (Kxx, Kyy, Kzz);
- porosity (θ).

No considerations were made regarding the geothermal gradient and the thermal flux because the model refers to the surface without significant thermal anomalies.

5.3. Thermo-Technical Model

Dealing with the thermo-technical model, double U-shaped geothermal pipes made of polyethylene material (PE100 RC) were placed inside each BHE (Figure 3), and their technical characteristics were defined in detail through the "borehole heat exchanger BC" tool. Their material and dimensions were based on the more commonly used pipes on the Italian market. Table 4 summarises the main input parameters of the BHEs used for this model.

Table 4. BHE characteristics. Key: L is the BHE length; D is the BHE diameter; d_{in} and d_{out} are the inner and outer pipe diameters; b_{in} and b_{out} represent the inner and outer pipe thicknesses; λ_{in} and λ_{out} are the inner and outer pipe thermal conductivities.

Pipe Configuration	L (m)	d_{in} (m)	b_{in} (m)	d_{out} (m)	b_{out} (m)	D (m)	λ_{in} (W*m^{-1}K^{-1})	λ_{out} (W*m^{-1}K^{-1})
Double U	60	0.026	0.0023	0.032	0.0029	0.15	0.42	0.42

The "borehole heat exchanger" tool was also used to set the fluid circulation inside each geothermal pipe. The fluid consisted of water with a flow rate of 40.0 m³/d corresponding to 0.46 l/s. The charging phase during the storage modality consisted of driving warm water at 70 °C (Tin) inside each circuit of the geometrical model (Figure 1) starting from the innermost BHEs towards the outermost ones. This kind of fluid circulation ensures the creation of the warmer core of the heat storage with lower losses into the environment. According to [39], temperatures up to 90 °C can be stored, using the BTES plant to store heat coming from renewable energy sources such as solar thermal. In our case study, a series of solar collectors scaled to produce a maximum of 70 °C were considered. A reverse fluid circulation was set, assuming a heat extraction phase from the warmer core during the colder months. In this case, fluid was injected at 15 °C from the outermost BHEs towards the innermost ones. This fluid temperature complied with the Italian laws regarding the classification and use of the geothermal resources. Two different scenarios were thus simulated, after an initial period of 4 months of charging the storage volume:

(i) a contribution to meet the base load through a continuous extraction over 30 days;
(ii) a contribution to meet peak demands through an intermittent energy exploitation.

6. Results

The results are shown for three different simulations: the first one is the charging phase between June and September as the best period for the BTES functionality, the others describe what happens during the two different kinds of energy extraction over a period of 30 days.

6.1. The Charging Phase

The simulations were conducted over 122 days corresponding to four months, covering the storage period between the spring and summer seasons.

The geometrical, hydrogeological, and thermo-technical models were applied, as previously described (Sections 5.1–5.3). Warm water at 70 °C was continuously injected (light blue line in Figure 5) in each circuit, while the ground temperature at the core of the system progressively increased.

In the first days, the temperature rose very fast in the reservoir; after that, the temperature increased slowly till the end of the simulation period (red line in Figure 5), recording a general outlet temperature of approximately 63 °C. Each circuit showed negligible differences, so that the outlet temperature (Tout) curves overlapped, taking on the aspect of a single line.
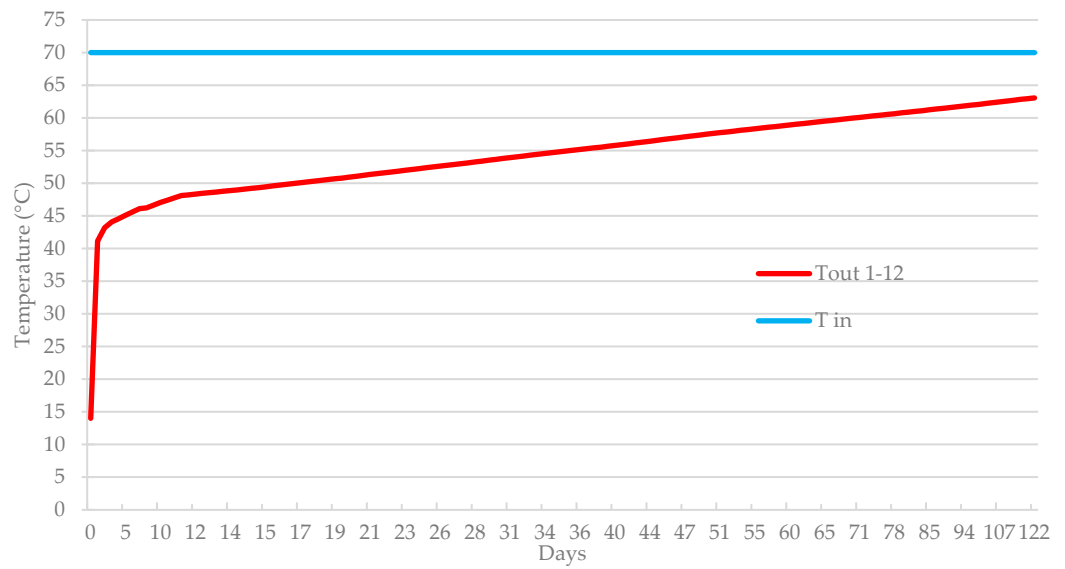
Figure 5. Inner (Tin, °C) and outlet (Tout, °C) temperatures over 122 days of operation of the BTES plant. The 12 considered fluid circuits of the model, where the overlap means the same thermal behaviour.

Figure 6 well defines the warmer core of the inner storage volume which did not exceed the 8 m radius from the centre (red/orange colours), progressively decreasing outwards, and reaching the original ground temperature of 14 °C. The BHE configuration and the layout of the circuits further ensured a perfect circular shape of the storage volume and of the thermal plume around it.
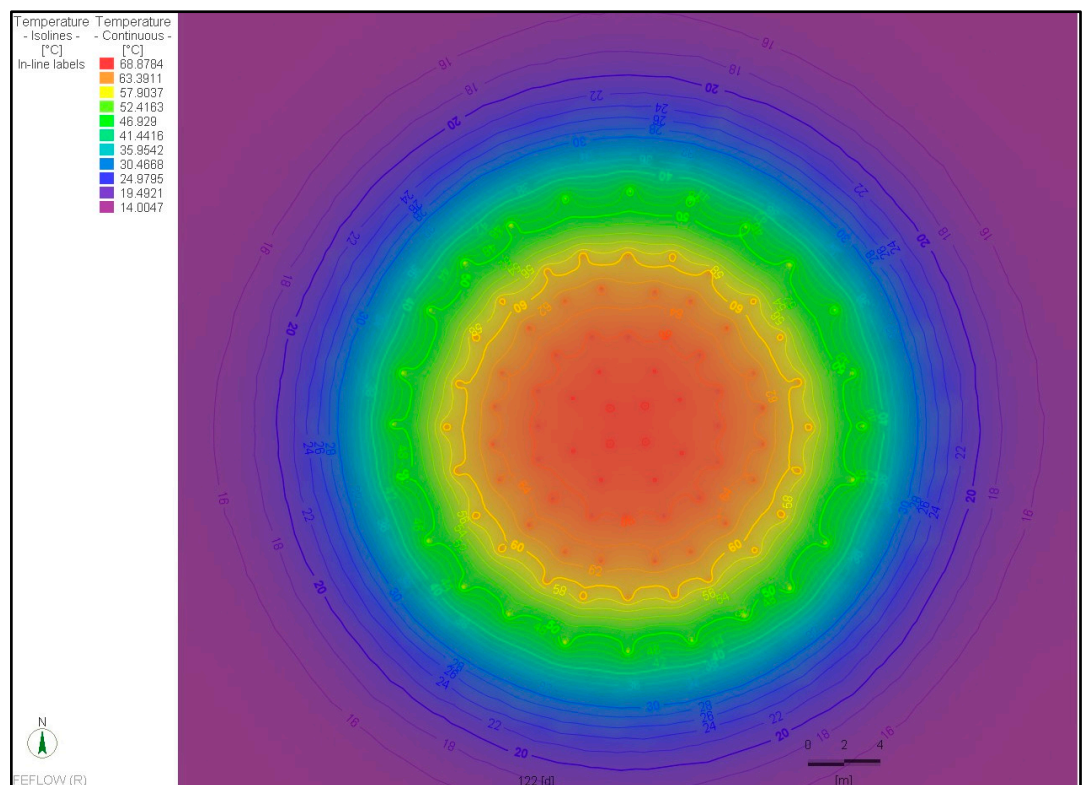

Figure 6. The 2D view of the ground thermal behaviour after 122 days of the storage plant operation.

6.2. Continuous Thermal Energy Extraction over 30 Days

Aimed at evaluating the ground thermal behaviour when the stored heat needs to be extracted for domestic use, a period of 30 days of heating (722 h) was taken into account. During the heat extraction, water at 15 °C was continuously injected in the outermost BHEs (blue light line, Figure 7), while ground temperature at the core of the storage system showed a sharp decrease: from 63 °C (representing the warm core of the storage volume) to 23 °C, which represents the outlet temperature (T_{out}) at the end of the heat extraction period (Figure 7). This resulted in a susbtantial depletion of the storage volume as represented in Figure 8.
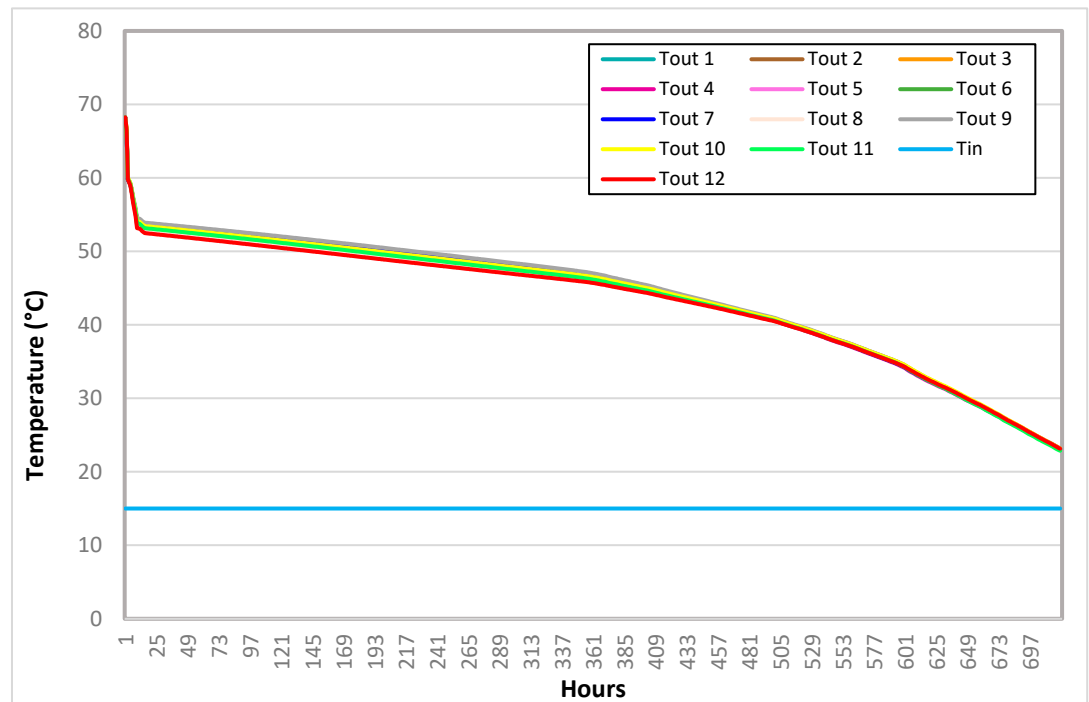

Figure 7. Inner (T_{in}, °C) and outlet (T_{out}, °C) temperatures over 30 days of operation in extraction modality, without switching off the plant. The 12 considered fluid circuits of the model overlap towards the end of the extraction phase, meaning more or less the same thermal behaviour.

In particular, in the first 10 days of operation (approximately 240 h), the outlet temperatures showed a slight decrease (temperature range between 55 °C and 46 °C, approximately) with the temperature curves recording a difference of a few tenths of a degree from each other. On the other hand, a steep decrease for all curves was instead shown in the last 10 days of the operation where a total overlap between curves is also displayed (Figure 7). A similar ground thermal behaviour could occur even in a longer period than those considered in these numerical simulations, avoiding a more significant cooling of the ground than its original temperature. This situation represents a continuous heat extraction without considering any interruption.
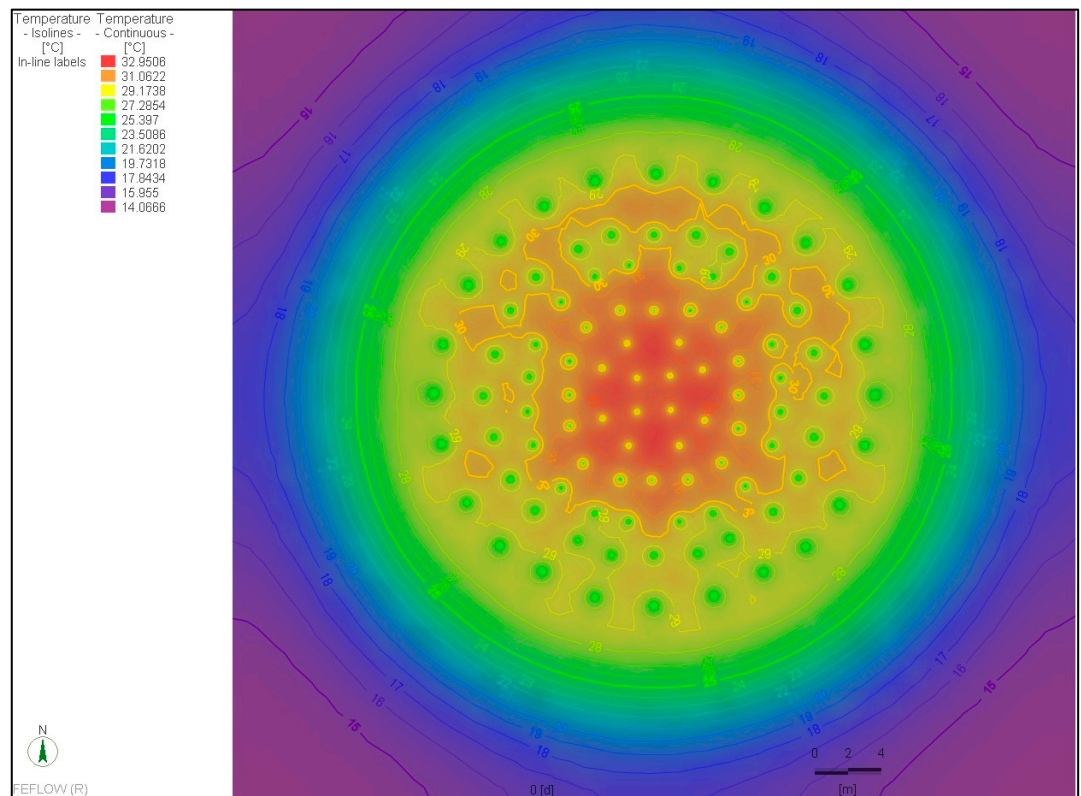
Figure 8. The 2D view of the ground thermal beahaviour after 30 days of continuous heat extraction from the storage system.

6.3. Intermittent Thermal Energy Extraction over 30 Days

The plant was set by switching it on 3 h per day (peak load) while switching it off for the remaining 21 h, thus assuming an intermittent use of the stored heat for a domestic use. A total period of 30 days of heating (722 h) was again taken into account; water at 15 °C was injected only during the plant operation for heating purposes.

During the heat extraction, the ground temperature showed a slight decrease over the considered period for each circuit which displayed a similar trend with negligible differences, starting from the original temperature equal to 63 °C (in the central inner portion of the storage volume) to 46.2 °C at the end of each circuit when the plant was totally switched off (Figure 9).

During each switch on/off cycle, a similar trend for the 12 circuits was maintained; a recovering of approximately 10 °C occured in the following hours when the plant was switched off.

Differently from the other case study (Section 6.2; Figure 8), at the end of the 30 days of heat extraction the original warm core of the storage system was still useable for a longer period, if necessary, by users. As represented in Figure 10, the warmer core of the original storage volume was kept within the 6 m radius from the centre (red/orange colours), progressively decreasing outwards and reaching the original ground temperature of 14 °C.
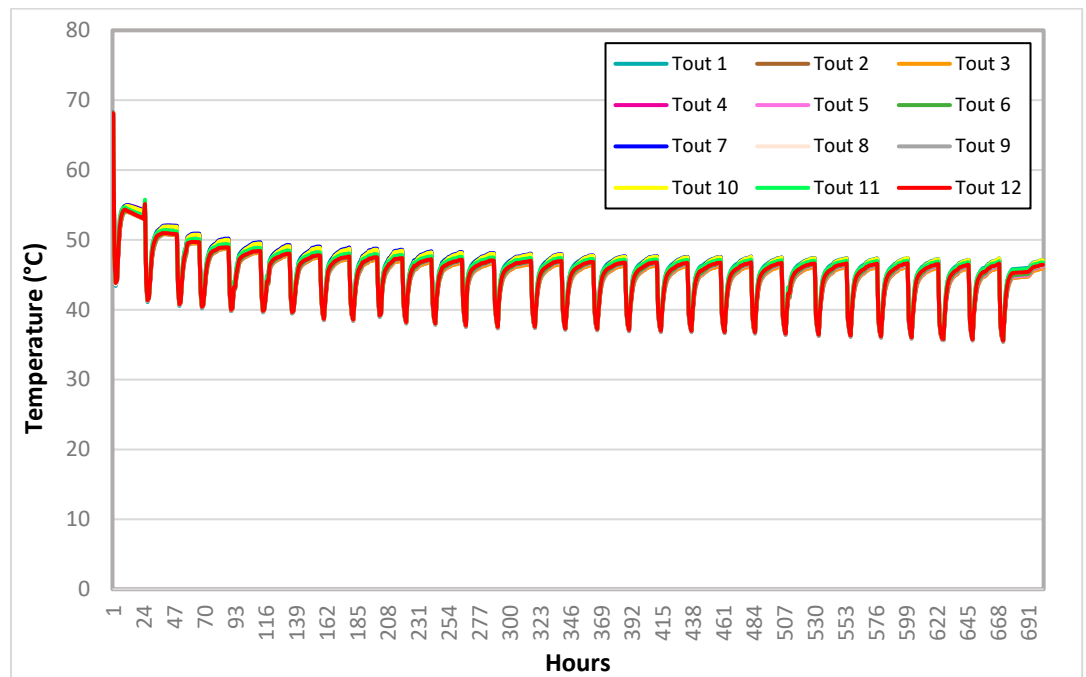
Figure 9. Inner (T_{in}, °C) and outlet (T_{out}, °C) temperatures over 30 days of operation in the extraction modality, switching on the plant for 3 h per day and switching it off the remaining 21 h. The 12 considered fluid circuits of the model displayed a similar trend with negligible differences.
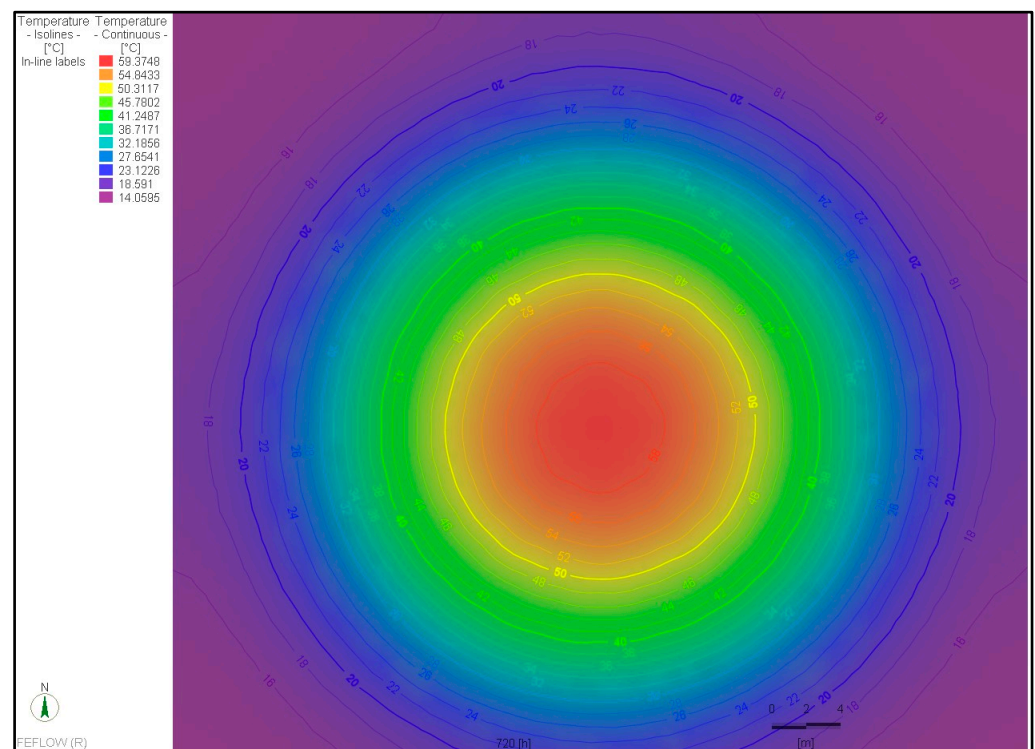

Figure 10. The 2D view of the ground thermal beahaviour after 30 days of intermittent heat extraction from the storage system.

7. Discussion

Regarding UTES technologies, the evaluation of their performance such as the storage efficiency and the thermal energy that can be extracted for space heating is of paramount importance in defining their techno-economic feasibility. This kind of evaluation helps to understand the advantages and drawbacks, improving the economic competi-

tiveness of UTES systems and providing a solid base for policy makers and investors [40]. To this regard, when evaluating the capital expenditure of these technologies (CAPEX), factors to be considered are drilling, storage piping, and all the other components which the system needs to operate as well as its storage efficiency. As highlighted in [10], in district heating and cooling (DHC) grids peak load systems are typically designed to have a low CAPEX with a higher operational expenditure (OPEX) as they are designed to run for only a limited time. To this regard, UTES technologies can reduce the amount of time peak load systems operate by using low-OPEX energy (e.g., from geothermal), and thus can be used to fill peak demand loads as well as to provide backup supply. UTES can also improve their overall performance, when connected to a DHC network as demonstrated in [41].

To assess the energy performance and to better understand the technical feasibility of UTES under design conditions, numerical simulations were revealed to be very useful. This is particularly true for BTES systems such as the one presented in this work, which is defined as one of the most popular and promising technologies for long-term storage [12,42]. The setup configuration of the studied BTES, with a total of 96 BHEs (more than the other technologies), spaced 2–3 m with a circular shape, can ensure a high storage capacity. Large arrays of BHEs at distances of a few metres, and in square, hexagonal, or circular shapes, allow, in fact, the efficient storage of heat. This means that the overall ratio between the volume and surface of the storage should be minimised [13].

As well, the sensitivity analyses (e.g., back analysis of the field GRT) proved to be a key factor in understanding in more detail the hydrogeological and thermo-physical characteristics as highlighted by several authors [30,43–45], and thus in assessing how the geological setting may affect the BTES [15,46]. Numerical simulations permitted optimisation of the storage capacity and efficiency of the designed BTES: the small temperature difference recorded between the warm water entering and leaving BHEs (Figure 5) for each circuit at the end of the storage period testifies to a good thermal energy distribution in terms of the heat injected, recovered, and stored. This also means that a circular configuration of BHEs and their arrays are more proper for ensuring a low percentage of heat loss during each circuit over the storage period and, thus, in assessing a great storage (Figure 6). The modelling showed that BTES can be used when the energy demand from users is greater than that produced by conventional heating systems, or when a failure in these systems occurs, acting as a sort of backup system. Therefore, knowledge of how to use the stored energy is a key factor in understanding how many users can exploit this energy source and thus how long the energy need can be satisfied. The thermal power (kW) and then the cumulative energy produced (kWh), as represented in Figures 11 and 12, can be obtained by multiplying the flow rate of the heat carrier fluid, its temperature when entering and leaving the BHEs for each circuit, and its specific heat capacity. In particular, a simplified equation of that reported in [47] can be used:

$$P = Q\,(T_{out} - T_{in}) * Cp \tag{3}$$

where P is the thermal power (W); Q is the heat flow rate (Kg/s); T_{out} and T_{in} (°C) are the inlet and outlet temperatures, respectively; and Cp is the specific heat capacity (J/Kg*°C).

Once the thermal power (P) was obtained, it was converted to kW and, thus, the cumulative energy E (kWh) was calculated over the considered period, using Equation (4):

$$E = \sum_{t\,(h)} P \tag{4}$$

where E is the cumulative energy (kW); P is the thermal power (kW); and t is the time (hour) at which each value of P was summed with the next one.
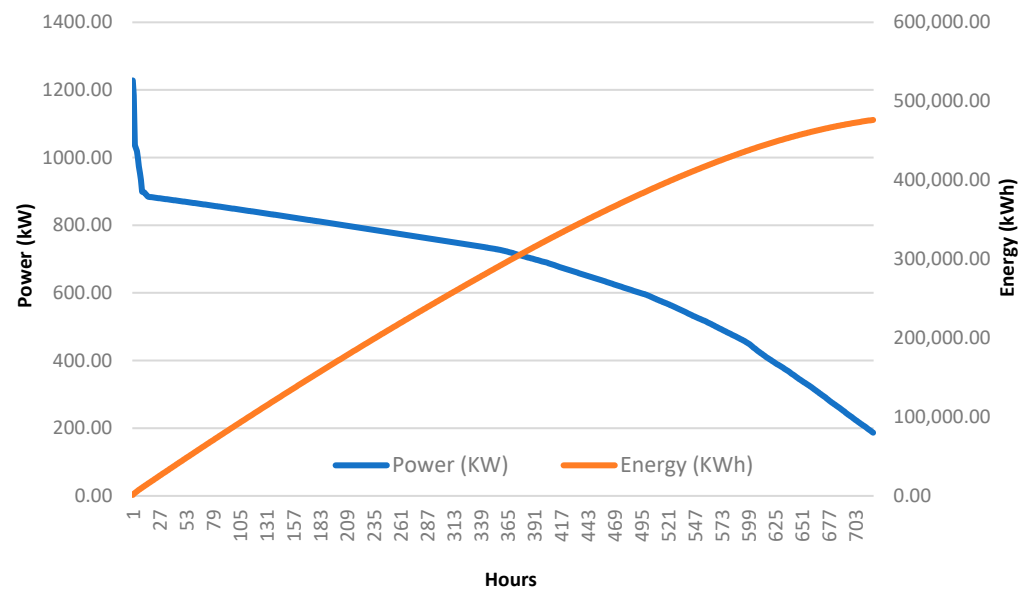
Figure 11. Power (kW) vs. energy (kWh), after 30 days of continuous heat extraction as shown in Section 6.2.
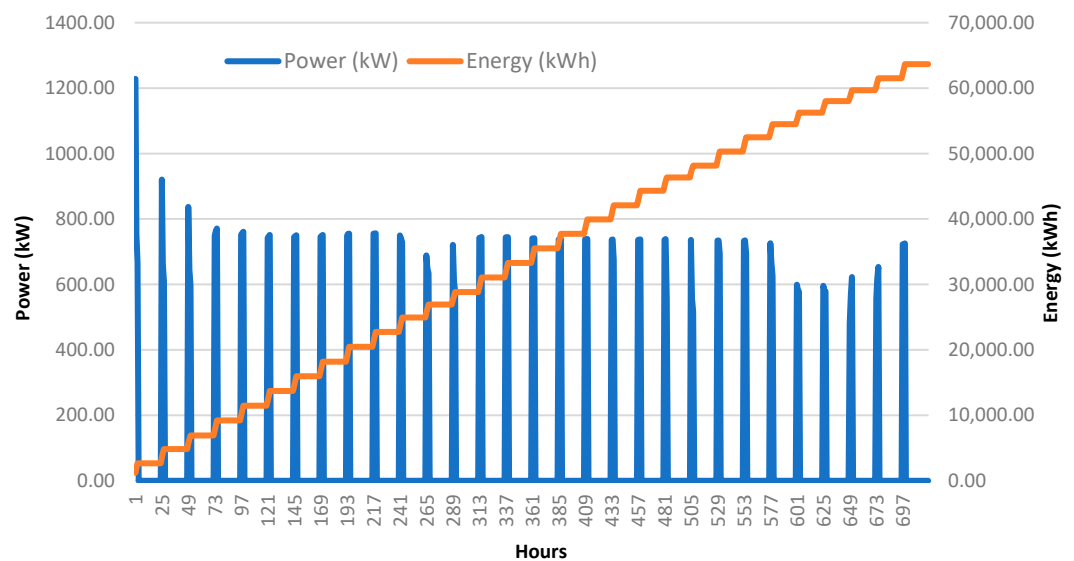

Figure 12. Power (kW) vs. energy (kWh), after 30 days of intermittent heat extraction as shown in Section 6.3.

In this framework, we assessed that a continuous extraction of the stored heat for heating purposes over a period of 30 days (722 h) would lead to a substantial depletion of the storage volume (Figure 8), meaning that the amount of energy stored is subjected to a strong decrease over time while the cumulative energy produced is growing strongly (up to 476,000 kWh; Figure 11). On the other hand, the intermittent use of the stored heat over the same period leads to a lower decrease in the stored thermal energy but also to less energy produced (up to 63,600 kWh) than in continuous use (Figure 12). This means that a continuous heat extraction from the storage volume can satisfy not only the base load but also the peak load supply of several users, especially when temporary failures in the heating system occur.

As represented in Figure 11, the thermal power strongly decreased over the first month of continuous use and, probably, a continuous heat extraction could satisfy the

energy needs of no longer than a few months in total. However, this is enough to feed the energy needs of several users in the case of an emergency and confirms, for example, how it is important to integrate UTES systems in DHC contexts.

Differently, when the stored heat is extracted only some hours per day the cumulative energy produced is much lower, but the thermal power of the original storage volume remains at higher values over at least the first month (Figure 12). This implies that the heat extraction in such a way can cover the energy needs of several months, filling the energy gap between the demand and production and satisfying peak loads.

8. Conclusions

Overcoming the mismatch between energy supply and demand promotes a faster decarbonisation of the future energy systems using smart approaches but is still a great challenge.

Existing and future district heating and cooling grids can be converted into multivalent networks, using different renewable energy sources such as solar thermal, photovoltaic, and geothermal not only for thermal energy production but also for storage purposes. This study proved that the integration of UTES systems can be an efficient solution to meet both base and peak loads requests, becoming an important provider of heating and cooling for buildings. Furthermore, these technologies can increase their efficiency if connected to a grid and thus meeting the thermal energy needs of several users.

The sensitivity analyses conducted in this work highlighted two main aspects:

- over the first month of continuous heat extraction (base load production), the cumulative energy amounted to 476,000 kWh, leading to a relevant depletion of the warm core; it resulted in a strong decrease in the available thermal power to be used for the following months (186.95 kW), and thus to a general decrease in the temperature inside the storage core of up to 23 °C, approaching the undisturbed ground temperature of 14 °C;
- if the heat extraction is planned for only some hours per day (peak load), the energy produced and usable for heating buildings is lower compared to when it is extracted continuously. It corresponded to 63,600 kWh, meaning a gradual reduction in the storage volume which maintains the original circular configuration. This means a greater amount of available thermal power to be exploited for heating purposes (725.36 kW) than the previous case. Therefore, the ground temperature at the warm core maintains high values at the end of the first month of extraction, recording a temperature difference of only 23.8 °C from the original storage temperature of 70 °C.

These results highlight that BTES systems are very flexible and are able to meet both peak and base loads following the request from the grid, also with the function of a backup system.

In summary, if properly sized, BTES technologies could be one of the most promising facilities for integration in DHC networks, because of their greater adaptability to all geological contexts as well as their higher storage capacity and efficiency.

References

1. IEA. Global Electricity Demand is Growing Faster than Renewables, Driving Strong Increase in Generation from Fossil Fuels. 2021. Available online: https://www.iea.org/news/global-electricity-demand-is-growing-faster-than-renewables-driving-strong-increase-in-generation-from-fossil-fuels (accessed on 31 October 2022).

2. UNFCC. The Paris Agreement. 2015. Available online: https://unfccc.int/sites/default/files/english_paris_agreement.pdf (accessed on 31 October 2022)

3. UNFCCC. Global Climate Action at COP26. 2021. Available online: https://unfccc.int/climate-action/gca-events/global-climate-action-at-cop-26 (accessed on 31 October 2022)

4. UNFCCC. Nationally Determined Contributions (NDCs); The Paris Agreement and NDCs (2022), United Nations Framework Convention on Climate Change. 2022. Available online: https://unfccc.int/ndc-information/nationally-determined-contributions-ndcs (accessed on 31 October 2022).

5. IEA. Defying Expectations, CO_2 Emissions from Global Fossil Fuel Combustion are Set to Grow in 2022 by only a Fraction of Last Year's Big Increase. 2022. Available online: https://www.iea.org/news/defying-expectations-co2-emissions-from-global-fossil-fuel-combustion-are-set-to-grow-in-2022-by-only-a-fraction-of-last-year-s-big-increase (accessed on 9 November 2022).

6. European Commission, 2019. A European Green Deal. Available online: https://ec.europa.eu/info/strategy/priorities-2019-2024/european-green-deal_en (accessed on 9 November 2022).

7. Goetlz, G.; Zosseder, K.; Vranjes, A.; Schifflechner, C.; Chicco, J.; Singh, R.M. Geothermal Heating and Cooling Networks for Green and Livable Urban Transformations—Part I, Sustainable European Cities and Digitization. *Eur. Now J.* **2021**. Available online: https://www.europenowjournal.org/2021/05/10/geothermal-heating-and-cooling-networks-for-green-and-livable-urban-transformations-part-i/ (accessed on 4 November 2022).

8. Heat Road Map Europe. Available online: https://heatroadmap.eu (accessed on 4 November 2022).

9. Mathiesen, B.V.; Bertelsen, N.; Schneider, N.; Sánchez-García, L.; Paardekooper, S.; Thellufsen, J.Z.; Djørup, S.R. *Towards a Decarbonized Heating and Cooling Sector in Europe: Unlocking the Potential of Energy Efficiency and District Energy*; Report; Department of Planning, Aalborg University: Aalborg, Denmark, 2019.

10. Chicco, J.M.; Antonijevic, D.; Bloemendal, M.; Cecinato, F.; Goetzl, G.; Hajto, M.; Hartog, N.; Mandrone, G.; Vacha, D.; Vardon, P.J. Improving the Efficiency of District Heating and Cooling Using a Geothermal Technology: Underground Thermal Energy Storage (UTES). In *New Metropolitan Perspectives*; Calabrò, F., Della Spina, L., Piñeira Mantiñán, M.J., Eds; NMP 2022; Lecture Notes in Networks and Systems; Springer: Cham, Switzerland, 2022; Volume 482, pp. 1699–1710. https://doi.org/10.1007/978-3-031-06825-6_164.

11. IEA. Very Large Thermal Energy Storage for Renewable Districts. 2021. Available online: https://www.iea.org/articles/very-large-thermal-energy-storage-for-renewable-districts (accessed on 31 October 2022).

12. Reuss, M. The use of borehole thermal energy storage (BTES) systems. In *Advances in Thermal Energy Storage Systems*; Elsevier: Amsterdam, The Netherlands, 2015; pp. 117–147. https://doi.org/10.1533/9781782420965.1.117.

13. Skarphagen, H.; Banks, D.; Frengstad, B.S.; Gether, H. Design Considerations for Borehole Thermal Energy Storage (BTES): A Review with Emphasis on Convective Heat Transfer. *Geofluids* **2019**, *2019*, 1–26. https://doi.org/10.1155/2019/4961781.

14. Lanahan, M.; Tabares-Velasco, P.C. Seasonal Thermal-Energy Storage: A Critical Review on BTES Systems, Modeling, and System Design for Higher System Efficiency. *Energies* **2017**, *10*, 743. https://doi.org/10.3390/en10060743.

15. Catolico, N.; Ge, S.; McCartney, J.S. Numerical Modeling of a Soil-Borehole Thermal Energy Storage System. *Vadose Zone J.* **2016**, *15*, 1–17. https://doi.org/10.2136/vzj2015.05.0078.

16. Boockmeyer, A. Numerical Simulation of Borehole Thermal Energy Storage in the Geological Subsurface. Ph.D. Thesis, Faculty of Mathematics and Natural Sciences at the Christian Albrechts University, Kiel, Germany, 2020. Available online: https://macau.uni-kiel.de/receive/macau_mods_00000629 (accessed on 4 November 2022).

17. Formhals, J.; Hemmatabady, H.; Welsch, B.; Schulte, D.; Sass, I. A Modelica Toolbox for the Simulation of Borehole Thermal Energy Storage Systems. *Energies* **2020**, *13*, 2327. https://doi.org/10.3390/en13092327.

18. Colucci, R.R.; Monegato, G.; Žebre; M. Glacial and proglacial deposits of the Resia Valley (NE Italy): New insights on the onset and decay of the last alpine glacial maximum in the Julian Alps. *Alp. Mediterr. Quat.* **2014**, *27*, 85–104. Available online: https://amq.aiqua.it/index.php/amq/article/view/75 (accessed on 4 November 2022).

19. Dosio, A.; Galmarini, S; Graziani, G. Simulation of the circulation and related photochemical ozone dispersion in the Po plains (northern Italy): Comparison with the observations of a measuring campaign. *J. Geophys. Res. Atmos.* **2002**, *107*, LOP-2. https://doi.org/10.1029/2000jd000046.

20. Viganò, A.; Zampieri, D.; Rossato, S.; Martin, S.; Selli, L.; Prosser, G.; Ivy-Ochs, S.; Campedel, P.; Fedrizzi, F.; Franceschi, M.; Rigo, M. Past to present deformation of the central-eastern Southern Alps: from the foreland to the Giudicarie belt. *Geol. F. Trips Maps* **2017**, *10*(1.1) (2018), 78. https://doi.org/10.3301/GFT.2018.01.

21. Scardia, G.; Festa, A.; Monegato, G.; Pini, R.; Rogledi, S.; Tremolada, F.; Galadini, F. Evidence for late Alpine tectonics in the Lake Garda area (northern Italy) and seismogenic implications. *GSA Bull.* **2015**, *127*, 113–130. https://doi.org/10.1130/b30990.1.

22. Zuccari, C.; Vignaroli, G.; Viola, G. Geological map of the San Donato—Costa Thrust Zone, Belluno Thrust System, eastern Southern Alps (northern Italy). *J. Maps* **2021**, *17*, 337–347. https://doi.org/10.1080/17445647.2021.1946444.

23. Cozzi, A. Synsedimentary tensional features in Upper Triassic shallow-water platform carbonates of the Carnian Prealps (northern Italy) and their importance as palaeostress indicators. *Basin Res.* **2000**, *12*, 133–146. https://doi.org/10.1046/j.1365-2117.2000.00117.x.

24. Monaco, P.; Giannetti, A. Three-dimensional burrow systems and taphofacies in shallowing-upward parasequences, lower Jurassic carbonate platform (Calcari Grigi, Southern Alps, Italy). *Facies* **2002**, *47*, 57–82. https://doi.org/10.1007/bf02667706.

25. Masetti, D.; Figus, B.; Jenkyns, H.C.; Barattolo, F.; Mattioli, E.; Posenato, R. Carbon-isotope anomalies and demise of carbonate platforms in the Sinemurian (Early Jurassic) of the Tethyan region: Evidence from the Southern Alps (Northern Italy). *Geol. Mag.* **2017**, *154*, 625–650. https://doi.org/10.1017/s0016756816000273.

26. Castellarin, A.; Vai, G.B.; Cantelli, L. The Alpine evolution of the Southern Alps around the Giudicarie faults: A Late Cretaceous to Early Eocene transfer zone. *Tectonophysics* **2006**, *414*, 203–223. https://doi.org/10.1016/j.tecto.2005.10.019.

27. Carminati, E.; Cavazza, D.; Scrocca, D.; Fantoni, R.; Scotti, P.; Doglioni, C. Thermal and tectonic evolution of the southern Alps (northern Italy) rifting: Coupled organic matter maturity analysis and thermokinematic modeling. *AAPG Bull.* **2010**, *94*, 369–397. https://doi.org/10.1306/08240909069.

28. Fleischmann, S.; Picotti, V.; Rugenstein, J.K.C.; Cobianchi, M.; Bernasconi, S.M. Effects of the Pliensbachian–Toarcian Boundary Event on Carbonate Productivity of a Tethyan Platform and Slope. *Paleoceanogr. Paleoclimatology* **2022**, *37*, e2021PA004392. https://doi.org/10.1029/2021pa004392.

29. Fredi, P.; Palmieri, E.L. Morphological Regions of Italy. In *Landscapes and Landforms of Italy. World Geomorphological Landscapes*; Soldati, M., Marchetti, M., Eds.; Springer: Cham, Switzerland, 2017; pp. 39–74. https://doi.org/10.1007/978-3-319-26194-2_5.

30. Francani, V.; Gattinoni, P. Hydrogeological aspects of Lombard Prealps karstification (northern Italy). *Ital. J. Eng. Geol. Environ.* **2009**, *1*, 117–135. https://doi.org/10.4408/IJEGE.2009-01.O-07.

31. Calligaris, C.; Boschin, W.; Cucchi, F.; Zini, L. The karst hydrostructure of the Verzegnis group (NE Italy). *Carbonates Evaporites* **2016**, *31*, 407–420. https://doi.org/10.1007/s13146-016-0320-7.

32. Eklöf, C.; Gehlin, S. Ted-a Mobile Equipment for Thermal Response Test: Testing and Evaluation. Master's Thesis, Luleå University of Technology, Luleå, Sweden, 1996; pp. 1–62. Available online: http://www.diva-portal.org/smash/get/diva2:1032479/FULLTEXT01.pdf (accessed on 4 November 2022).

33. Mogensen, P. Fluid to duct wall heat transfer in duct system heat storages. In Proceedings International Conference on Subsurface Heat Storage in Theory and Practice, Stockholm, Sweden, 6–8 June 1983; pp. 652–657

34. Raymond, J.; Mercier, S.; Nguyen, L. Designing coaxial ground heat exchangers with a thermally enhanced outer pipe. *Geotherm. Energy* **2015**, *3*, 7. https://doi.org/10.1186/s40517-015-0027-3.

35. Javed, S.; Spitler, J. Calculation of Borehole Thermal Resistance. In *Advances in Ground-Source Heat Pump Systems*; Woodhead Publishing: Cambridge, UK, 2016; Volume 1, pp. 63–95, ISBN 9780081003114.

36. Claesson, J.; Dunand, A. *Heat Extraction from the Ground by Horizontal Pipes: A Mathematical Analysis*; BFR Documents; Byggforskningsrådet (BFR): Stockholm, Sweden, 1983. Available online: https://lucris.lub.lu.se/ws/portalfiles/portal/4375488/8146470 (accessed on 4 November 2022).

37. Chicco, J.M.; Mandrone, G. How a sensitive analysis on the coupling geology and borehole heat exchanger characteristics can improve the efficiency and production of shallow geothermal plants. *Heliyon* **2022**, *8*, e09545. https://doi.org/10.1016/j.heliyon.2022.e09545.

38. Diersch, H.-J. G. Using and testing the algebraic multigrid equation solver SAMG in FEFLOW. *FEFLOW White Pap.* **2009**, *3*, 25–36.

39. Sibbitt, B.; McClenahan, D. Seasonal Borehole Thermal Energy Storage—Guidelines for Design & Construction. International Energy Agency—Solar Heating & Cooling Programme 2015. pp. 1–15. Available online: https://task45.iea-shc.org/data/sites/1/publications/IEA-SHCT45.B.3.1-TECH-Seasonal-storages-Borehole-Guidelines.pdf (accessed on 4 November 2022).

40. Yang, T.; Liu, W.; Kramer, G.J.; Sun, Q. Seasonal thermal energy storage: A techno-economic literature review. *Renew. Sustain. Energy Rev.* **2021**, *139*, 110732. https://doi.org/10.1016/j.rser.2021.110732.

41. Xu, L.; Torrens, J.I.; Guo, F.; Yang, X.; Hensen, J.L. Application of large underground seasonal thermal energy storage in district heating system: A model-based energy performance assessment of a pilot system in Chifeng, China. *Appl. Therm. Eng.* **2018**, *137*, 319–328. https://doi.org/10.1016/j.applthermaleng.2018.03.047.

42. Panno, D.; Buscemi, A.; Beccali, M.; Chiaruzzi, C.; Cipriani, G.; Ciulla, G.; Di Dio, V.; Brano, V.L.; Bonomolo, M. A solar assisted seasonal borehole thermal energy system for a non-residential building in the Mediterranean area. *Sol. Energy* **2019**, *192*, 120–132. https://doi.org/10.1016/j.solener.2018.06.014.

43. Gehlin, S.E.A.; Hellstrom, G. Comparison of Four Models for Thermal Response Test Evaluation. *ASHRAE Trans. Atlanta* **2003**, *109*, 131. Available online: https://www.diva-portal.org/smash/record.jsf?pid=diva2%3A991442&dswid=-3191 (accessed on 4 November 2022).

44. Loveridge, F.; Holmes, G.; Roberts, T.; Powrie, W. Thermal response testing through the Chalk aquifer in London, UK. *Proc. Inst. Civ. Eng. Geotech. Eng.* **2013**, *166*, 197–210. https://doi.org/10.1680/geng.12.00037.

45. Zhang, C.; Guo, Z.; Liu, Y.; Cong, X.; Peng, D. A review on thermal response test of ground-coupled heat pump systems. *Renew. Sustain. Energy Rev.* **2014**, *40*, 851–867. https://doi.org/10.1016/j.rser.2014.08.018.

46. Li, P.; Guo, F.; Yang, X. An inversion method to estimate the thermal properties of heterogeneous soil for a large-scale borehole thermal energy storage system. *Energy Build.* **2022**, *263*, 112045. https://doi.org/10.1016/j.enbuild.2022.112045.

47. Kuosa, M.; Rahiala, S.; Tallinen, K.; Mäkilä, T.; Lampinen, M.; Lahdelma, R.; Pulkkinen, L. Mass flow controlled district heating with an extract air heat pump in apartment buildings: A practical concept study. *Appl. Therm. Eng.* **2019**, *157*, 113745. https://doi.org/10.1016/j.applthermaleng.2019.113745.